Supporting Information: The Role of Fe Species on NiOOH in Oxygen Evolution Reactions

Yecheng Zhou*,†,‡ and Núria López*,‡

†*School of Materials Science & Engineering, Sun Yat-Sen University, Guangzhou 510275 Guangdong, P. R. China.*

‡*Institute of Chemical Research of Catalonia (ICIQ), The Barcelona Institute of Science and Technology (BIST), Av. Països Catalans, 16, 43007 Tarragona, Spain*

E-mail: zhouych29@mail.sysu.edu.cn; nlopez@iciq.es

Contents

1 Pourbaix diagram

1.1 Free energy and reaction energy calculation details

Except *ab initio* molecular dynamics (AIMD) simulations, all of other calculations were performed by VASP[S1] with a planewave cutoff energy of 750 eV. The calculated valence electron configurations for Ni, O, H and Fe are $3d^8 4s^2$, $2s^2 2p4$, $1s^1$ and $3d^6 4s^2$, respectively. Γ centred K-mesh with K point distance less than $2\pi/45$ $\mathring{A}^{-1}$ was employed for solid phases. For gas phases, only Γ point was used. The Hubbard U correction is applied for PBE calculations. According to previous investigations,[S2–S6] the U value of nickel and iron are set to be 5.5 and 3.3, respectively. U term is aimed to described the interaction of d electrons of transition metal oxides, which is structure sensitive. Hence, the U parameter should vary from one compound to others. The same U for all compound for the PBE+U calculations may be problematic. But if we use different U for different compounds, it is also problematic because the formation energy is calculated

by $E(form) = E_{total} - \sum_i E_{atom}$. Energies are not comparable if they are calculated by different calculation settings. As illustrated in the Table S1, for some compounds their energies significantly change, while others change very little. As for the metal phase nickel, no U parameter is required, the formation energy calculated by different U may be meaningless. Therefore, we use a more advanced calculation method - HSE06 to repeat all calculations, which does not involve empirical parameters. The data shown in the main paper are HSE06 results.

Table S1: Total energies of various compound calculated with different U parameters test for nickel.

			Intrinsic		
Compounds	U=4.5	U=5.5	U=6.5	Diff(5.5-4.5)	Diff(6.5-5.5)
NiO	-10.432	-10.271	-10.134	0.162	0.136
Ni3O4	-36.296	-35.466	-34.698	0.830	0.768
Ni2O3	-98.715	-96.222	-94.130	2.493	2.092
NiO2	-15.038	-14.534	-14.053	0.504	0.481
NiOOH	-20.258	-19.868	-19.590	0.390	0.278
Ni(OH)2	-25.325	-25.158	-25.015	0.167	0.143
			Doped		
Compounds	U=4.5-3.3	U=5.5-3.3	U=6.5-3.3	Diff(5.5-4.5)	Diff(6.5-5.5)
NiO	-251.507	-248.064	-245.179	3.443	2.885
Ni3O4	-289.527	-283.428	-277.862	6.098	5.566
Ni2O3	-299.273	-293.979	-288.921	5.293	5.058
NiO2	-358.340	-347.050	-336.073	11.289	10.978
NiOOH	-486.654	-478.557	-471.870	8.097	6.687
Ni(OH)2	-608.804	-605.238	-602.215	3.566	3.023

Free energy of all compounds are calculated by:

$$G_x(T) = E_x + ZPE_x - (S_x - C_x)T \tag{1}$$

where, G_x is the free energy of compound x, E_x is the DFT total energy calculated by VASP, ZPE is the Zero Point Energy calculated by Phonopy 1.13 (only the bulk phases in this part, the ZPE of gas molecules and reaction intermediates are calculated by VASP),[S1] and S_x and C_x are the entropy and the heat capacity, which are also calculated by Phonopy. Entropies and heat capacities of H_2(gas), H_2O(gas), O_2(gas) are obtained from National Institute of Standards and Technology, USA (NIST Standard Reference

Database 13, https://janaf.nist.gov). Due to large errors in the GGA+U calculation of O_2 bonding energy,[S7,S8] the reference O_2 energy are also calculated by $G_O = G_{H_2O} + 2.46\,eV - G_{H_2}$ (U= 0 V and pH=0). The enthalpy of O_2 difference between direct calculated by DFT and HSE06 and abstracted from H_2O are 0.60 eV and 0.21 eV, respectively. Initial ferro magnetic orders were set here.

1.2 Free energy and reaction energies

Formation energies of compounds are obtained by $G_f(x) = G_x - \sum_i \mu_i$, where μ_i is the free energy of pure element i at its lowest energy configuration. For example, $\mu_O = 0.5 * G_{O_2}$. $\mu_{Ni} = G_{Ni}/n_{Ni}$, where G_{Ni} is the total free energy of Ni cell and n_{Ni} is the number of Ni ions in the cell. The reaction free energy change is defined by $\Delta G = \sum_{product} G - \sum_{reactant} G$. Free energies of ions are abstracted from experiments in ref. S9.

Table S2: Experiment and DFT energies and enthalpies of H_2, O_2, H_2O. All unit is eV. Contribution of $(C_p - S) * T$ is sourced from https://janaf.nist.gov. ZPE is estimated from frequency calculation of VASP.

Molecules	PBE E	HSE06 E	$(C_p - S) * T$	ZPE	G_{therm}	G_{PBE}	G_{HSE06}
H_2	-6.773	-7.654	-0.316	0.282	-0.034	-6.807	-7.688
O_2	-9.872	-14.240	-0.546	0.101	-0.445	-10.318	-14.685
$O_2(H_2O)$	-9.272	-14.028	-0.546	0.101	-0.445	-9.717	-14.474
H_2O	-14.217	-17.476	-0.483	0.574	0.091	-14.126	-17.385

Table S3: Phonopy calculated thermal related parameters of $Ni_xO_yH_z$ before doping. Energy units are eV.

Compounds	ZPE	S300	C300	F300	DG((S-C)T)	ZPE-DG	N_{fml}/cell	GT/fml
Ni	0.039	0.000	0.000	0.001	0.013	0.026	1	0.026
NiO	0.180	0.001	0.001	0.026	0.052	0.129	1	0.129
NiO_2	0.507	0.001	0.001	0.416	-0.071	0.578	2	0.289
Ni_3O_4	0.868	0.003	0.003	0.487	0.001	0.866	2	0.433
Ni_2O_3	1.259	0.004	0.004	0.746	-0.020	1.279	4	0.320
NiOOH	0.384	0.000	0.001	0.322	-0.023	0.407	1	0.407
$Ni(OH)_2$	0.763	0.001	0.001	0.673	-0.006	0.769	1	0.769

Table S4: Phonopy calculated thermal related parameters of $Ni_xO_yH_z$ after doping. Energy units are eV.

Compounds	ZPE	S300	C300	F300	DG((S-C)T)	ZPE-DG	N_{fml}/cell	GT/fml
Ni	0.902	0.003	0.003	0.504	-0.005	0.907	24	0.038
NiO	2.118	0.009	0.008	0.957	0.126	1.992	24	0.083
NiO_2	1.836	0.009	0.007	0.610	0.360	1.477	24	0.062
Ni_3O_4	4.302	0.007	0.008	3.467	-0.412	4.713	8	0.589
Ni_2O_3	4.816	0.005	0.006	4.252	-0.365	5.181	12	0.432
NiOOH	11.422	0.010	0.013	10.189	-0.769	12.191	24	0.508
$Ni(OH)_2$	19.388	0.014	0.016	17.660	-0.638	20.025	24	0.834

1.3 Considered reactions

To plot the Pourbaix diagram, phase boundaries have to been determined through reactions. Each reaction defines one transition boundary of two phase. There are two reactions (reaction 11 and reaction 22, shown in Table S5), which can not be shown Pourbaix as there is no H^+ or e^- involved in these reaction. However, these two reactions demonstrate which is more stable between $Ni(OH)_2$ and NiO, or, Ni_2O_3 and NiOOH. We found that energy of 2 unit of NiOOH always has lower energy than that of an unit Ni_2O_3 and a H_2O molecule. This indicates that Ni_2O_3 is a meta-stable phase of NiOOH.

Table S5: Considered reactions to plot Pourbaix diagram.

Reactions
$Ni \longrightarrow Ni^{2+} + 2\,e^-$
$Ni + 2\,H_2O \longrightarrow Ni(OH)_2 + 2\,H^+ + 2\,e^-$
$Ni + 4\,H_2O \longrightarrow Ni(OH)_4{}^{2-} + 4\,H^+ + 2\,e^-$
$Ni^{2+} + 2\,H_2O \longrightarrow Ni(OH)_2 + 2\,H^+$
$Ni^{2+} + H_2O \longrightarrow Ni(OH)^+ + H^+$
$Ni^{2+} + 2\,H_2O \longrightarrow NiO_2 + 4\,H^+ + 2\,e^-$
$Ni^{2+} + 2\,H_2O \longrightarrow NiOOH + 3\,H^+ + e^-$
$Ni(OH)_2 + H^+ \longrightarrow Ni(OH)^+ + H_2O$
$Ni(OH)_2 + H_2O \longrightarrow Ni(OH)_3{}^- + H^+$
$Ni(OH)_2 + 2\,H_2O \longrightarrow Ni(OH)_4{}^{2-} + 2\,H^+$
$Ni(OH)_2 \longrightarrow NiOOH + H^+ + e^-$
$Ni(OH)_2 \longrightarrow NiO_2 + 2\,H^+ + 2\,e^-$
$Ni(OH)_2 \longrightarrow NiO + H_2O$
$3\,Ni(OH)_2 \longrightarrow Ni_3O_4 + 2\,H_2O + 2\,H^+ + 2\,e^-$
$2\,Ni(OH)_2 \longrightarrow Ni_2O_3 + H_2O + 2\,H^+ + 2\,e^-$
$NiOOH \longrightarrow NiO_2 + H^+ + e^-$
$Ni(OH)_4{}^{2-} + H^+ \longrightarrow NiOOH + 2\,H_2O + e^-$
$Ni(OH)_4{}^{2-} \longrightarrow NiO_2 + 2\,H_2O + 2e^-$
$Ni_3O_4 + 2\,H_2O \longrightarrow 3\,NiO_2 + 4\,H^+ + 4\,e^-$
$Ni_3O_4 + 2\,H_2O \longrightarrow 3\,NiOOH + H^+ + e^-$
$Ni_3O_4 + 8\,H^+ + 2\,e^- \longrightarrow 3\,Ni^{2+} + 4\,H_2O$
$Ni_3O_4 + 8\,H_2O + 2\,e^- \longrightarrow 3\,Ni(OH)_4{}^{2-} + 4\,H^+$
$2\,NiOOH \longrightarrow Ni_2O_3 + H_2O$
$NiO + 2\,H^+ \longrightarrow Ni^{2+} + H_2O$
$NiO + 2\,H^+ + 2\,e^- \longrightarrow Ni + H_2O$
$NiO + 3\,H_2O \longrightarrow Ni(OH)_4{}^{2-} + 2\,H^+$
$NiO + 2\,H_2O \longrightarrow Ni(OH)_3{}^- + H^+$
$3\,NiO + H_2O \longrightarrow Ni_3O_4 + 2\,H^+ + 2\,e^-$
$2\,NiO + H_2O \longrightarrow Ni_2O_3 + 2\,H^+ + 2\,e^-$
$NiO + H_2O \longrightarrow NiO_2 + 2\,H^+ + 2\,e^-$
$NiO + H_2O \longrightarrow NiOOH + H^+ + e^-$

1.4 Pourbaix diagram comparison of PBE+U and HSE06

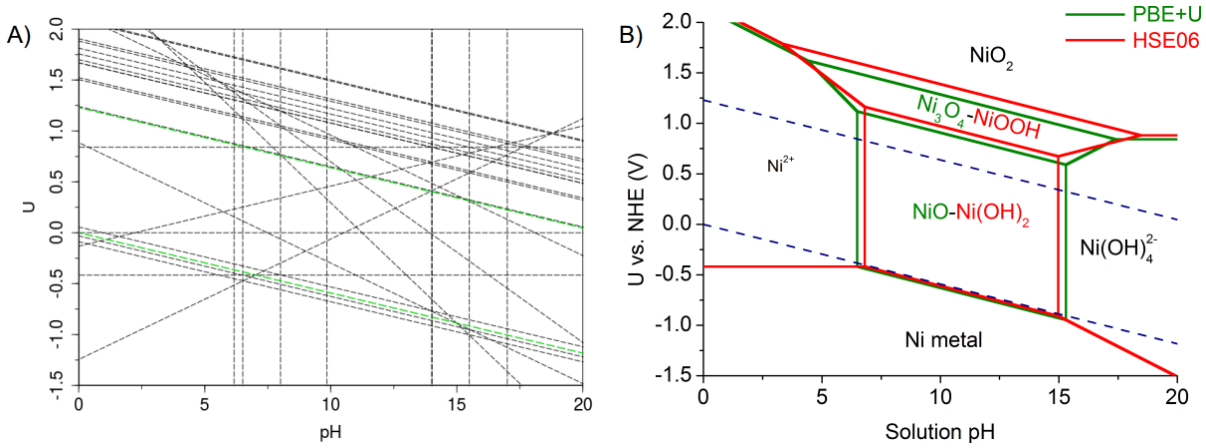

Figure S1: A) Lines considered to plot the Pourbaix diagram of Nickel-water system calculated by PBE+U. Each line is where the reaction heat of one chemical reaction equals zero. It is the phase boundary of the reactant phase and the product phase. In the regions near lines, the energy of the reactant phase and the product phase are very close. One present as the stable phase, the other should may also exist as a meta stable phase. Based on this logic, there are lots of metastable at the region of U .vs. SHE $\in$ (1.5 V,1.9 V). B) Pourbaix diagram of Nickel-water system calculated by PBE+U and HSE06.

2 Calculation details of surface energy

2.1 Surface energies in vacuum and solutions

Two methods have been performed to calculate the surface energy. The first is building two symmetric surfaces and then fully relaxed. The surface energy can be expressed by

$$G_{rlx}(surface) = (E_{rlx}(surface) - nE(bulk))/2,$$

where $E(bulk)$ is the total energy of a unit $NiOOH$ in its bulk, and $E_{rlx}(surface)$ is the energy of the configuration with two symmetric fully relaxed surfaces. The method is noted with subscript "rlx".

The second method is that one calculates the energy of unrelaxed two surface at first, then the energy of unrelaxed surface is estimated by

$$G_{fix}(surface) = (E_{fix}(surface) - nE(bulk))/2.$$

After that, we fix one surface and relax the other surface, and then calculate the total energy. Finally, the surface energy can be obtained by

$$G_{fix-rlx}(surface) = E_{rlx}(surface) - G_{fix}(surface) - nE(bulk)$$

Surface energies considered the solvent effect are also calculated with two different methods: VASP-SOL[S10] and VASP-MGCM.[S11]

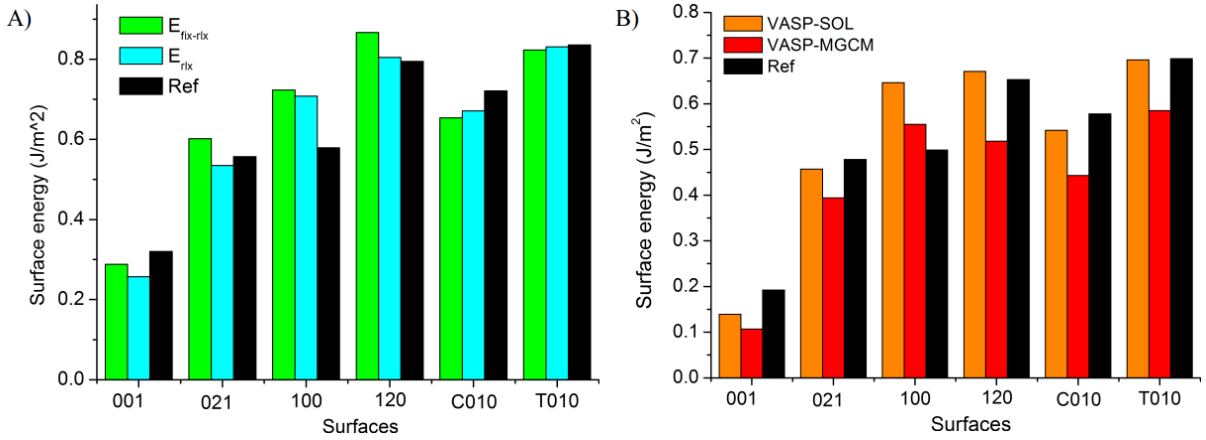

Figure S2: Surface energies of various NiOOH surfaces in vacuum A) and in water solution B) with two different method.

The surface energies of (001), (100), $(\bar{1}20)$, $(C010)$, $(T010)$ and (021) surfaces, corresponding to (0001), $(10\bar{1}0)$, $C-(01\bar{1}0)$, $T-(01\bar{1}0)$ and $(01\bar{1}1)$ surfaces in ref. S12, have been calculated by two different surface models. The calculated surface energies are shown Figure S2. VASP-SOL, developed by Prof. Hennig's group, aims to implement the solvent effect into surface calculation.[S10] Our group has also developed an alternative one, VASP-MGCM, which shows better consistence with Gaussian 09.[S11] The (001) surface is the most stable surface no matter in vacuum or in solution.

(001) surfaces with various H_2O coverages, and intercalated models with same amount H_2O molecules are simulated. The built unit cell with surface area of 30.2 $Å^2$ covered with or intercalated with 1, 2, 3, 4 H_2O molecules have been simulated. A short time of AIMD simulations for all models were performed in order to obtain the most possible water intercalation and adsorption configurations. Snapshots with low energy then were abstracted. It was found that the water configuration are similar in these low energy

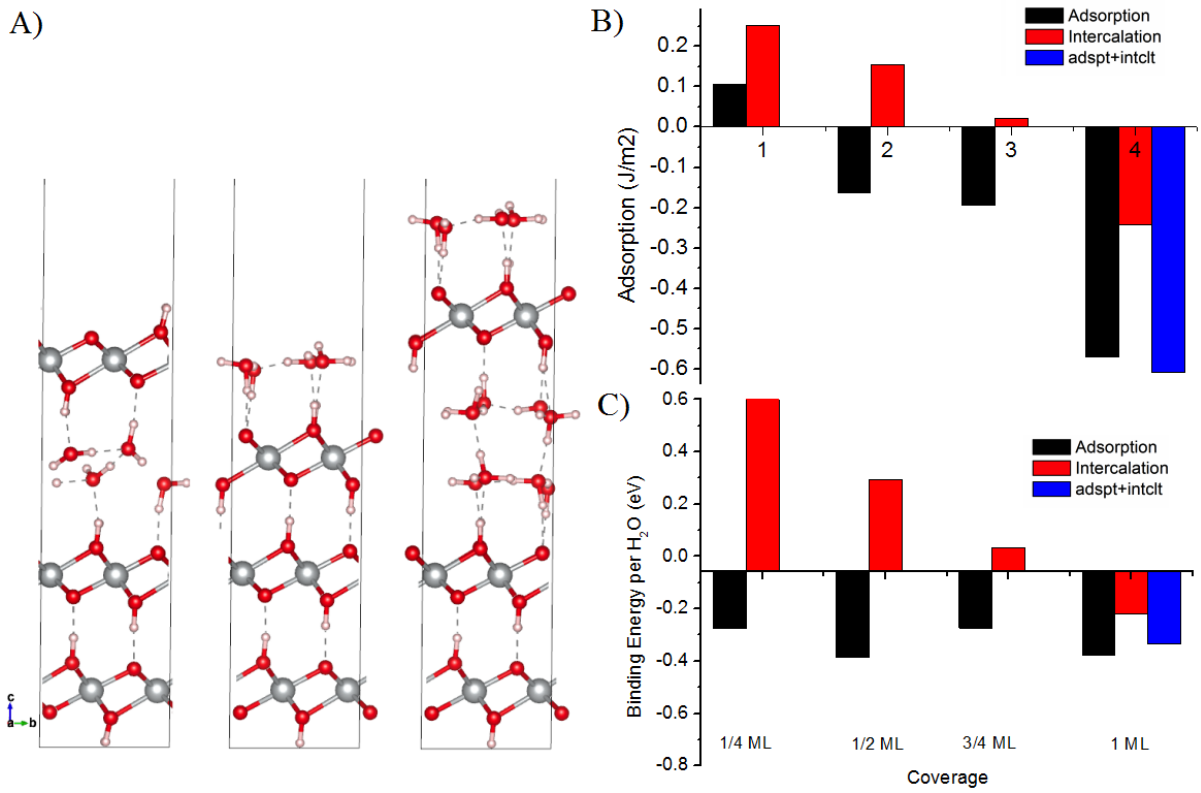

Figure S3: A) Adsorption and intercalation model: 4 H_2O molecules on (001) surface; 4 H_2O molecules intercalated in layers; 8 H_2O molecules intercalated in layers and 4 H_2O molecules on 001 surface. B) surface energies and C) binding energies of adsorption and intercalation models.

snapshots. The snapshot with lowest energy in the similar configurations were relaxed, and then their static energies were calculated. It is found that H_2O is very easy to adsorb on the surface, with adsorption energy of ≈ -0.27 eV, as shown in Figure S3C). The intercalation energy of H_2O diverse. It is an energy cost process if only a few of H_2O intercalated in layers per 30.2 $Å^2$. However, intercalation becomes energy favorable if 4 H_2O are intercalated into layers. With the help of H_2O, so-called the negative surface energy is realized at high density adsorption and intercalation, which suggests that the surface will spontaneously form and become layer-layer structure, the same to the porous structure happens in θ-Al_2O_3.[S13] We further intercalated more water and formed two water layers, which more hydrogen bonds form. This will result in lower energy to -0.55 eV, which close to the surface adsorption energy. These results indicate the intercalation of water molecules are energy feasible, which is comparable to water adsorption. Therefore, water molecules can go into layers, then increase electrodes volume, agrees with the observed volume expansion under OER working conditions.[S14]

3 Formation energies of Fe doping possible configurations

The formation energies are calculated by:

$$E_{form} = E_{adspt} - (E_{intrinsic} + E_{cluster})$$

and

$$E_{form} = E_{intclt} - (E_{intrinsic} + E_{cluster}).$$

Please mind that, for the most model, the connection of cluster and surface produces H_2O molecules, for example, the adsorption model the Fe ion replace the surface H and leave a OH^-. The replaced H and leaved OH^- form a H_2O and adsorbs on the surface. The calculation processes is elucidated in Figure S4.

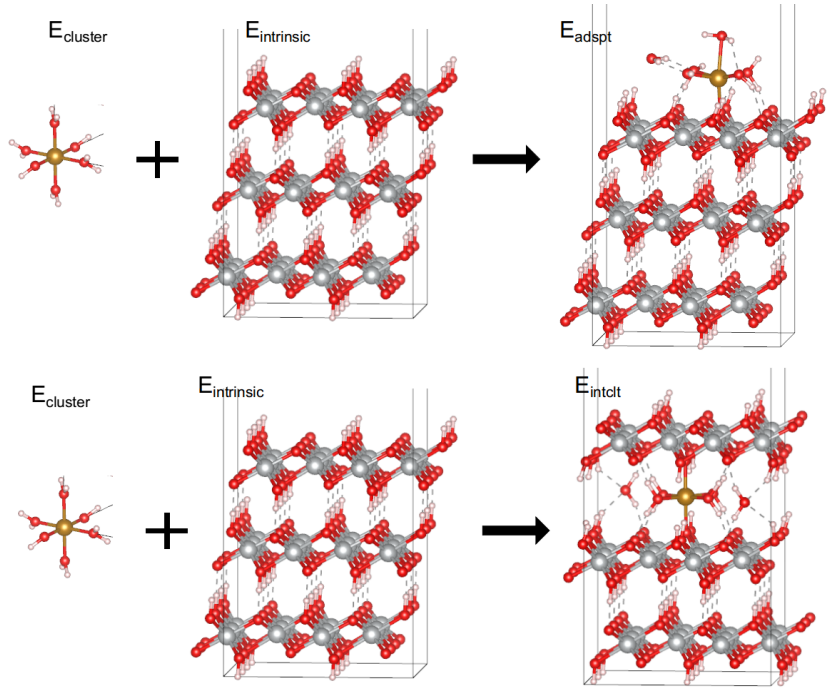

Figure S4: Calculation of formation energies. The connection of a Fe ion and a NiOOH surface will produce a H_2O.

Before constructing explicit doping configurations, we discuss the possibility of forming Fe dimers. Energy of Fe ions and their dimer are calculated, which found out that the separated Fe ion has lower energy than corresponding dimer, indicated by Table S6. Hence, there should be no Fe ion clusters in solution.

Table S6: Energy and Formation energies of Fe ions and their dimers. Energy units are eV.

Species	Formula	E(eV)	E $2H_2O$(eV)	Sum E(eV)	Two separated Fe ions
H_2O	H_2O	-14.235			
Fe^{2+}	$H_{10}O_6Fe$	-85.264			
Fe^{3+}	H_9O_6Fe	-81.205			
Fe^{2+}-dimer	$H_{16}O_{10}Fe_2$	-140.389	-28.470	-168.859	-170.528
Fe^{3+}-dimer	$H_{14}O_{10}Fe_2$	-132.223	-28.470	-160.693	-162.410

If Fe ions prefer in its monomer form, then there are several possible doping configurations:

- No interaction, NiOOH keeps its lattice, Fe is still in its free ion form.

- Ion exchange. The Fe ion replace a Ni ion in the lattice. This is the most discussed model in theory and experiment.
- Adsorption. Fe ions adsorbed on the NiOOH surface.
- Intercalation. Fe ions intercalated in two NiOOH layers.
- Mix of ion exchange and Ni ion adsorption. Fe ion exchanges with lattice Ni and Ni ion adsorb on the doped surface.

All this configurations were shown in Figure S5. By calculating their formation energies (Table S7), we found out that the adsorption models (include the mix models) are the most energetically favorable. The strong adsorption of the Fe^{2+} indicates that this configuration should be very stable. The bonding energy of Fe^{3+} is about half of Fe^{2+}. Surprisingly, the most assumed and discussed ion exchange has almost the highest formation energy. The possibility of Fe cluster forming were also discussed by estimating the formation energy of Fe-Fe dimer adsorption. Fe^{3+} dimer adsorption formation energy is about -2.86 eV, which is lower than the energy (-2.15 eV) of two Fe ion adsorbed separately. But this energy difference may be compensated by entropy as separated Fe ions have more adsorption possibilities. Additionally, the Fe^{2+} has lower energy. Thus, mono-Fe ions cluster adsorbed on the surface should be the most possible case in reaction conditions. The mixed of ion exchange and adsorption of Ni seems have lowest energy, but its formation should start with ion exchange, which is not energy favorable, or start with Fe^{2+} adsorption and then exchange Fe^{2+} and Ni^{3+}, which involves lots of bond breaking, high energy barrier is expected. The stability of these configurations are also proved by later AIMD simulations.

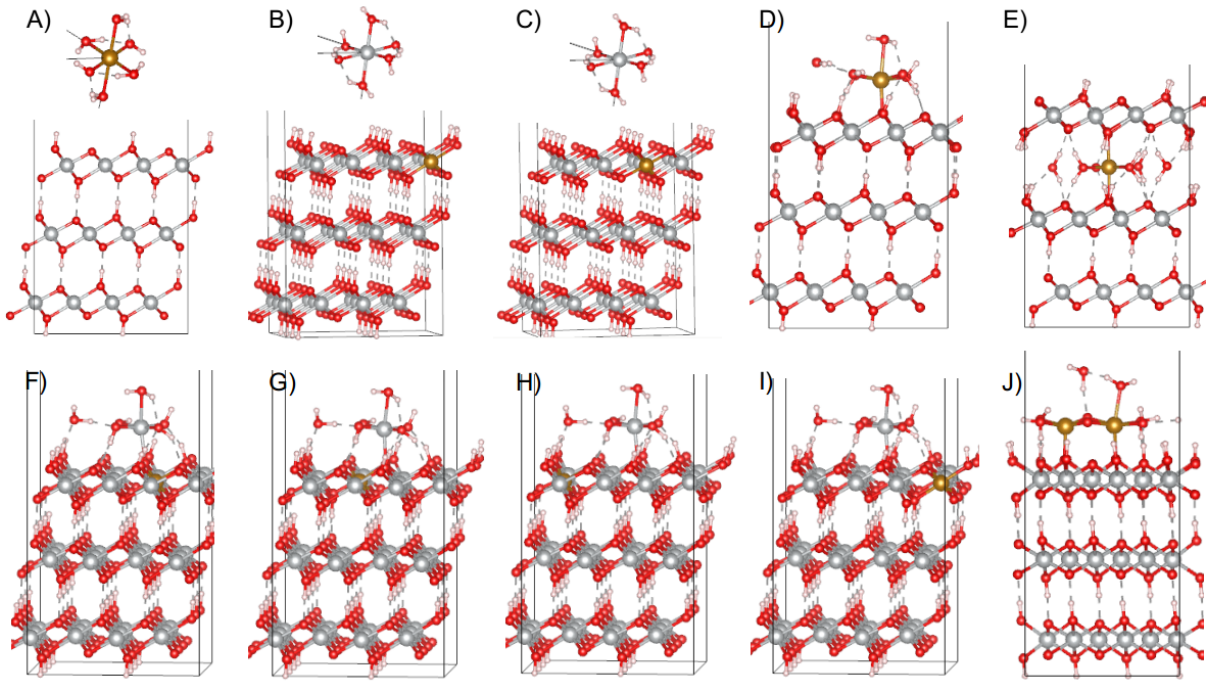

Figure S5: Possible Fe^{3+} doping configurations: A) no interaction; B)-C) ion exchange; D) adsorption; E) intercalation; F)-I) Ion exchange and Ni ion adsorption with different Fe doping sites; J) Fe-Fe dimer adsorption.

Table S7: Formation energies of possible Fe doping configurations. Their structures are shown in Figure S5 with corresponding labels. Energy units are eV. Please mind that the OS states of ions are the initial OS, it may increase by transferring a proton from coordinated H_2O to the surface O and becoming OH^-.

Doping structures	Label	Fe^{3+}	Fe^{2+}
Free iron ion	A	0.000	0.000
Ion exchange	B	1.701	-0.127
Ion exchange	C	1.590	-0.238
Adsorption-Octahedral[a]	D	-1.236	-2.543
Adsorption-Tetrahedral	NONE	-1.201	-2.490
Intercalation[b]	E	-0.088	-1.142
Mix-F	F	-1.320	-2.874
Mix-G	G	-1.213	-2.741
Mix-H	H	-0.961	-2.572
Mix-I	I	-1.056	-2.650
FeO_6H_x dimer	J	-1.422(-2.86)[c]	-2.088(-3.53)[d]

[a] The adsorption model of Fe^{2+} and Fe^{3+} are the relaxed 2UP and 3UP model, respectively. [b] The Intercalation model of Fe^{2+} and Fe^{3+} are the relaxed 2IN6 and 3IN6 model, respectively. [c] The energy of hydrogen bond of generated H_2O is ignored. Considering $4H_2O$ may form 8 hydrogen bonds, lead to about 4*0.36=1.44 eV lower in energy of -2.86 eV, which is 0.4 eV lower than isolated Fe^{3+} adsorption. [d] The $Fe-O_2-Fe$ connection of requires two electrons for each oxygen ion, four in total. But bonding with the surface also needs one election. Two hydrogen was added to the two connecting oxygen ions in order to keep Fe ion in 2+. The value in bracket is corrected by considering the hydrogen bonding energy.

4 AIMD simulations

4.1 Calculation details

The AIMD simulations were performed by CP2K 5.0[S15] with the Quickstep method and the PBE+U functionals. The energy cutoff was 280 Ry, snapshots were saved every 10 steps. At the beginning, a time step about 0.3 fs (some times convergence problems occur, we then changed it to 0.299 fs) was used. After a certain period time, the time step was increased to be 1 fs. Short time step at the beginning was used to avoid the dramatical change and convergence problems due to large forces in the initial structures. The layer-layer distance (D_{LL}) is calculated by the difference between the average z coordinates of Ni ions in upper and bottom layers.

4.2 AIMD model construction

The AIMD model is built on a three layer NiOOH (001) surface with surface area of 8.84 × 10.30 Å. It is a 3 × 2 supercell of (001) surface of NiOOH. The NiOOH surface structure was cleaved from the MC2 bulk structure in Ref. S12. A monolayerH_2O in 3×3 array can fully cover the surface.

Table S8: Number of $H_2O(OH^-)$ molecules in AIMD models. The result in the manuscript is from models with more H_2O under the condition that the all Fe-O(lattice) bonds are not broken.

Models	SET 1		SET 2	
	N_{H2O}(free)	N_{H2O}(total)	N_{H2O}(free)	N_{H2O}(total)
2IN6, 3IN6, 2IN7 and 3IN7	3(4)*	7(8)	6	10
2UP and 3UP	8	13	14	19
2IN10 and 3IN10	8	13	14	19
BRIDGE	6	8	15	19
TILT	9	12	15	19

The number of water molecules my play a role in other parameters. To avoid such problem two actions have been taken: a) iron ions in all models are fully coordinated, which ensures that the first solvation sphere condition is the same; b) two sets of models with different numbers of water molecules and sizes of gaps were built to assess the role of extra water. In principle, the number of embedded H_2O can vary according to the

layer-layer distance. So, we tried two sets of models, one set of models try to keep the Fe-O(lattice) bond connected, the other set of models should have more H_2O that make sure Fe ions are fully coordinated and the $Fe(OH_x)_y$ clusters are surrounded with H_2O. Due to different surfaces and intercalation spaces, it is impossible to use the same number of water molecules for all models. However, the procedure to build our models is generally the same: they contain either a monolayer H_2O adsorption model or two-layer H_2O adsorption model.The particular numbers were listed in Table S8.

For the intercalation models with oxidation state (OS) initially in Fe^{2+} and Fe^{3+} (2IN6 and 3IN6 models), we removed 6 H_2O from a monolayer H_2O intercalated model to place a $Fe(OH)_x(H_2O)_{4-x}{}^{2-}$. The initial interlayer distance of 2IN6 and 3IN6 are around 6 Å. We built the 2IN7 and 3IN7 models, which have the same number of water molecule with 2IN6 and 3IN6 but the initial interlayer distance is 7 Å. We also built 2IN10 and 3IN10 models by removing H_2O in the two-layer H_2O intercalated model. Due to more H_2O, the initial layer-layer distance is 10 Å. Compared to the first set of models, the second set of models have the same layer-layer distance but one more layer of H_2O compacted in the gap. It is found that this extra layer H_2O will enlarge the gap and broke the Fe-O(lattice) bonds. Therefore, we could conclude that more H_2O were embedded, a bigger gap will open.

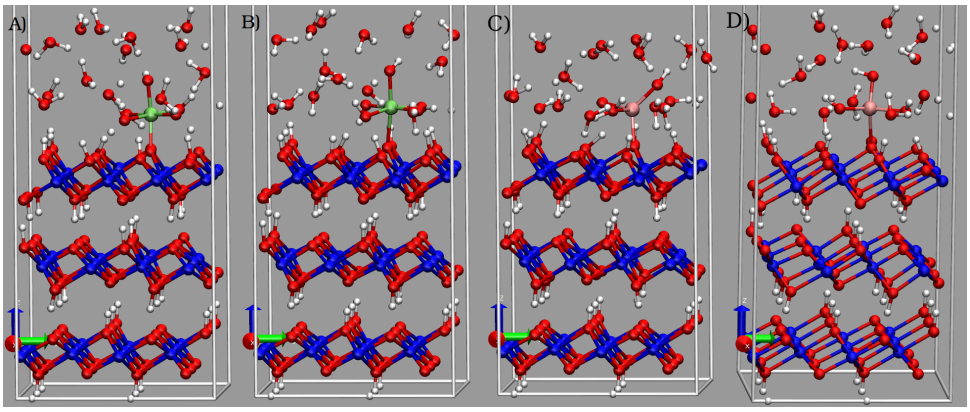

Figure S6: Adsorption models for AIMD simulations: A) the 2UP model. The initial oxidation state (OS) of the Fe ion is 2+. The Fe ion coordinates with 4 H_2O and OH^-. B) the 3UP model, the initial OS of the Fe ion is 3+. The Fe ion coordinates with 3 H_2O and 2 OH^-. C) the 2UP-Tetra model. The initial oxidation state (OS) of the Fe ion is 2+. The Fe ion coordinates with 2 H_2O and OH^-. D) the 3UP-Tetra model, the initial OS of the Fe ion is 3+. The Fe ion coordinates with 1 H_2O and 2 OH^-.

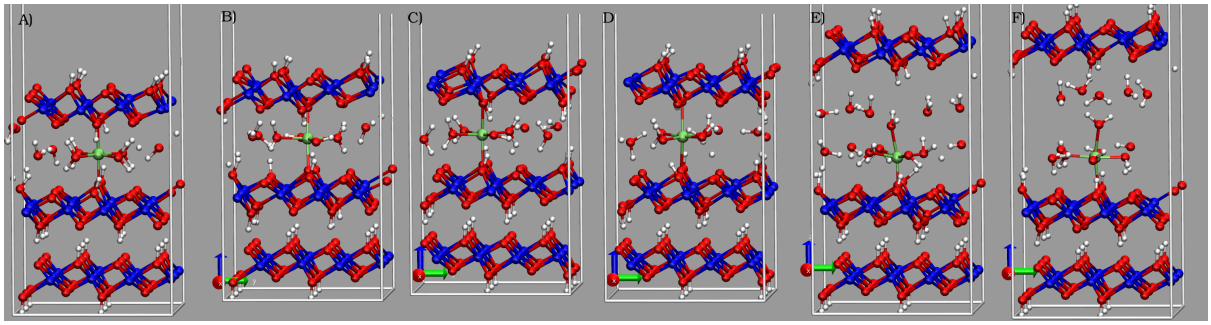

Figure S7: Intercalation models with one Fe ion for AIMD simulations: A) 2IN6, a Fe^{2+} is clipped in layers with initial layer-layer distance about 6 Å. Fe ion connects both upper and bottom layer, and 4 H_2O. B) 3IN6, a Fe^{3+} is embedded in layers with initial layer-layer distance about 6 Å. Fe ion connects both upper and bottom layer, and 3 H_2O and one OH^-. C) 2IN7, a Fe^{2+} is intercalated in layers with initial layer-layer distance about 7 Å. D) 3IN7, a Fe^{3+} is sandwiched in layers with initial layer-layer distance about 7 Å. E) 2IN7, a Fe^{2+} is placed in layers with initial layer-layer distance about 10 Å. F) 3IN7, a Fe^{3+} is placed in layers with initial layer-layer distance about 10 Å.

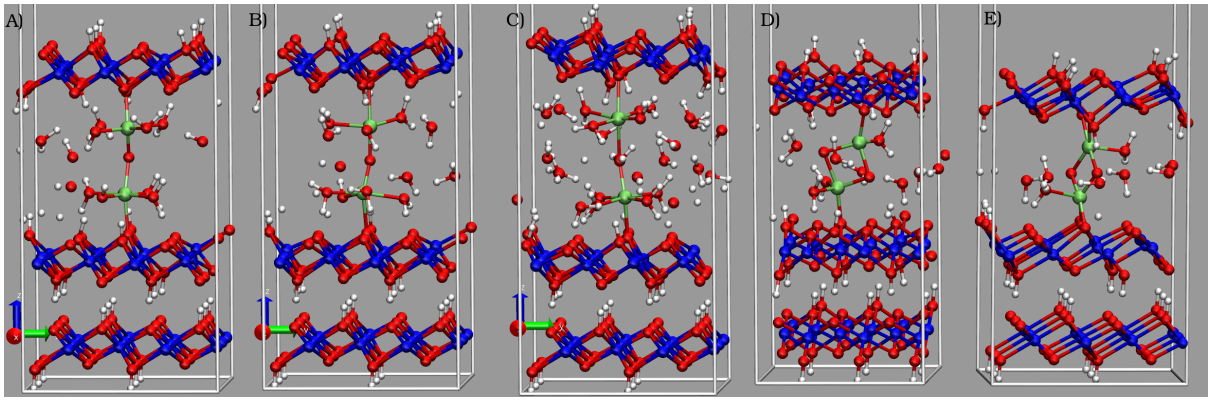

Figure S8: Intercalation models with two Fe ions for AIMD simulations: A) 2FE2, two Fe^{2+} are intercalated in layers. Each Fe ion coordinates with one surface and 4 H_2O. An oxygen ion connects these two Fe^{2+}. B) 2FE3, two Fe^{3+} are intercalated in layers. Each Fe ion coordinates with one surface, 3 H_2O and OH^-. An oxygen ion connects these two Fe^{3+}. C) FE2FE3, one Fe^{2+} and one Fe^{3+} are intercalated in layers. Fe^{2+} coordinates with one surface and 4 H_2O. Fe^{3+} coordinates with one surface, 3 H_2O and one OH^-. These two Fe ions are connected by an oxygen ion. D) TILT, the intercalation model with two iron ions bonded by two oxygen ions of the surface. E) BRIDGE, intercalation model with two iron ions connected through two oxygen ions, and each iron ion is coordinated to two surface oxygen ions.

4.3 Coordination number calculation

The coordination number(CN) of iron ions is determined by the Fe-H_2O or Fe-OH dimer relative energies. It is calculated by:

$$CN = \sum_i \frac{E_{max} - E(x_i)}{E_{max} - E_{min}} \tag{2}$$

where E_{max} is the energy Fe-H_2O dimer with distance of cutoff (3 Å). Dimers with distances higher than this cutoff distance are not considered as coordination. E_{min} is the minimum energy among all Fe-H_2O dimers. The distance of the Fe-H_2O dimer with minimum energy is set as the lower limit. Dimers with distances shorter than this lower limit contribute an unit to CN. The energy is calculated by $E(x) = 0.21755092 * (2.1/x)^{12} - 0.21487934 * (2.1/x)^6 - 0.32068992 * (2.1/x)^3 - 17.54733434$, which is fitted from DFT results. As shown in Figure S9, the Stockmayer potential, which adds a dipole term on the Lennard-Jones(LJ) potential, shows better fitting. Hence, the Stockmayer potential was used in this work.

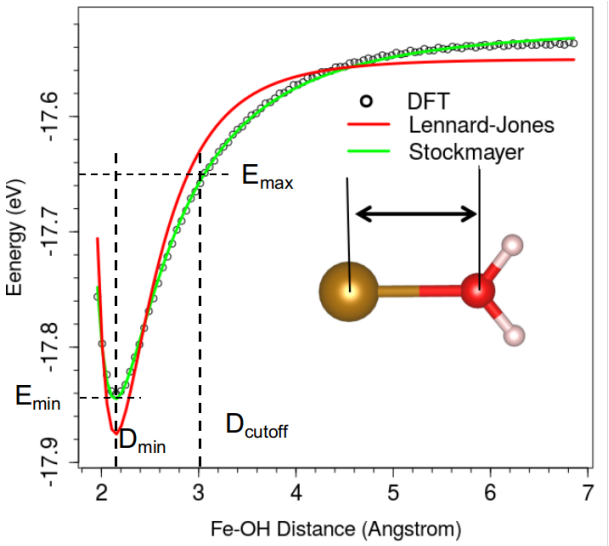

Figure S9: DFT calculated Fe-OH energies and fitting of Lennard-Jones and Stockmayer potentials.

4.4 Fe oxidation state calculation

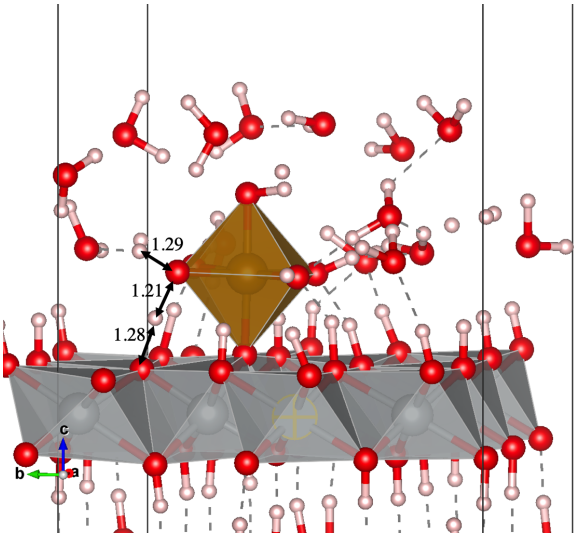

Figure S10: Snapshot of 2UP model at 27 fs. A H ion locates between the O coordinated with iron ion and the O of the lattice surface. It is difficult to determine which O atom does this H belong to.

We tried to use traditional method to calculate the OS of Fe, but none of them gives correct values. The Bader charge is unable to describe the OS of an ion if polarization and electrostatic orbital overlap contribute to the charge distribution.[S16] As we have shown in Table S12-Table S14, although the reaction happens, the Bader charges of these active site change very little. Hence, Bader charge is invalid here.

Traditionally, the OS of Fe is calculated by counting the coordinated OH^- groups. One OH^- group contributes 1+ to the OS of Fe ion. But there is a problem to determine whether the coordinated O is a OH^- group or H_2O. Figure S10 demonstrated a snapshot of 2UP model at 27 fs. A H atom is near to the O of bottom NiOOH surface and the O coordinated with iron ion. It is not obvious which O atom deos the H exactly belong to. This indicates that the electron of H is shared by the O of bottom NiOOH surface and the O coordinated with iron ions. Hence, the traditionally method to determine the OS of Fe by counting the number of coordinated OH^- group is not reasonable.

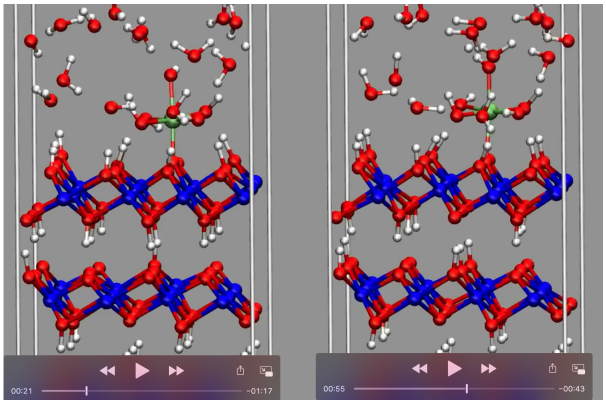

Figure S11: Snapshots of 2UP models. some H of H_2O coordinated with Fe were transferred to the NiOOH surface.

On the other hand, in some cases, some H of H_2O coordinated with Fe were transferred to the NiOOH surface, the coordinated H_2O becomes OH^-, which will contribute +1 more to the iron ion Figure S11. Figure S12 demonstrates the calculated OS of Fe ion in the 2UP model. The bottom bar is the OS calculated by traditional method. The main species Fe calculated by transitional method are very high OS, such Fe^{5+} and Fe^{6+}, which are not possible under mild chemical conditions. Therefore, we think the transferred H on the surface also provide some electrons to the Fe cluster and lower the OS of iron ion. Here, we define: $OS(Fe) = \sum w_{OH} + 0.5$. 0.5 is the contribution from the lattice O where Fe is adsorbed on. w_{OH} is the OH^- weight of coordinated OH_x groups. Traditionally, w_{OH} is a unit if the coordinated O is part of a OH^- group, and it is zero if the coordinated O belongs to a H_2O. As we cannot tell whether the H belongs to the coordinated O or the lattice surface O, we cannot determine it is a OH^- group or a H_2O. Here, based on the O-H distance(D), we calculated the weight of a H that contributes to the corresponding O.

$$\begin{aligned} w_H &= 1, D \leq D_{min}; \\ w_H &= \frac{E(D_{cut}) - E(D)}{E(D_{cut}) - E(D_{min})}, D_{min} < D \leq D_{cut} \end{aligned} \tag{3}$$

where, $E_{min} = E(D_{min})$ is the energy of the Stockmayer potential profile at a distance near the minimum, and $E_{cut} = E(D_{cut})$ is the Stockmayer potential of H locating at the cutoff distance. In this case, neither LJ nor Stockmayer can give good fitting (Fig-

ure S13A). We only take the part that we are interested to fit (Figure S13B), where the fitting is reasonable.

Then, the OH^- contribution can be calculated by $w_{OH} = 2\sum w_H$. For example:

- If a H is closely bonded with O ($D \leq D_{min}$), this H contribute one H to the O ($w_H = 1$). If there is another H also closely connected, it also contributes one to this O ($w_H = 1$). Then, for this O: $w_{OH} = 211 = 0$, which means it is H_2O, not contribution to the OS of Fe;

- If only one H is closely coordinated with this O, then $w_{OH} = 2 - 1 = 1$, it is a OH^- group. This OH^- group will contribute +1 to the OS of Fe;

- If there are two H coordinated with this O, their weights are 0.8 and 0.6, respectively. Its $w_{OH} = 2 - 0.8 - 0.6 = 0.6$, which means this O will contribute +0.6 to the OS of Fe.

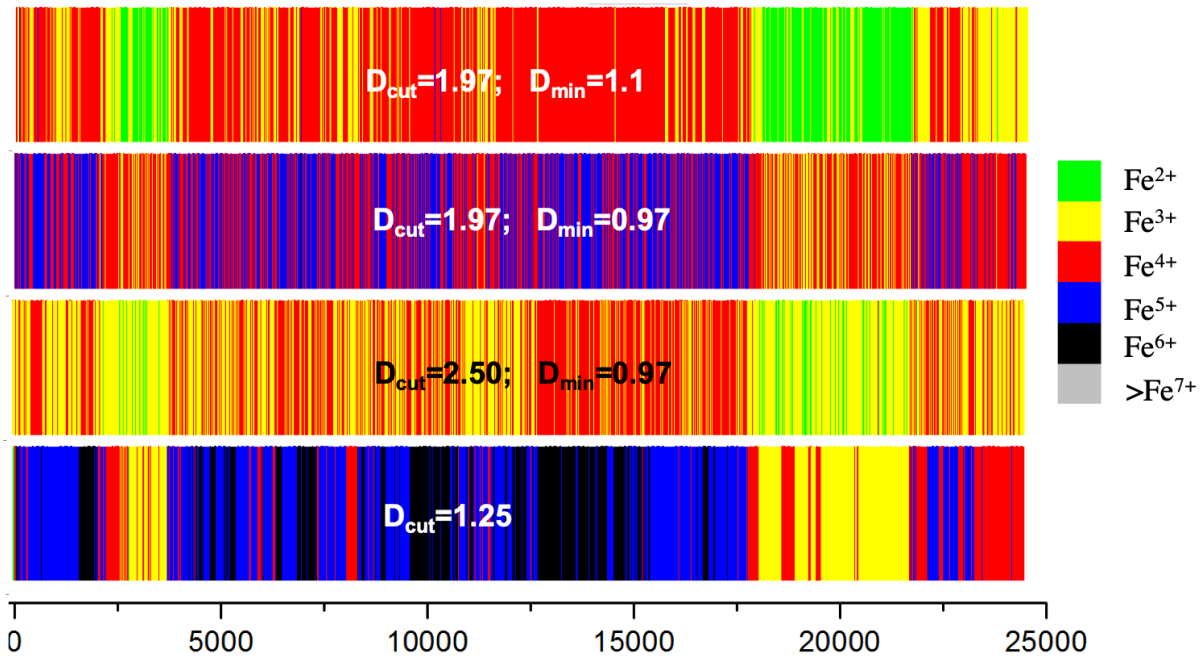

Figure S12: Snapshot of 2UP model at 27 fs. A H ion locates between the O coordinated with iron ion and the O of the lattice surface. It is difficult to determine which O atom this H belongs to.

Other three bars in Figure S12 are OSs calculated by our method with different cutoff distances and minimum distances. Our methods give much more reasonable OS compared

to the traditional method. By testing parameters, we chose D_{cut}=1.97 Å and D_{min}= 1.1 Å , because this set value looks more reasonable and also these two distances have physical meaning: 1.97 Å is hydrogen bond length in water and 1.1 Å is where the error between DFT data and fitting line is shapely reduced (Figure S13B).

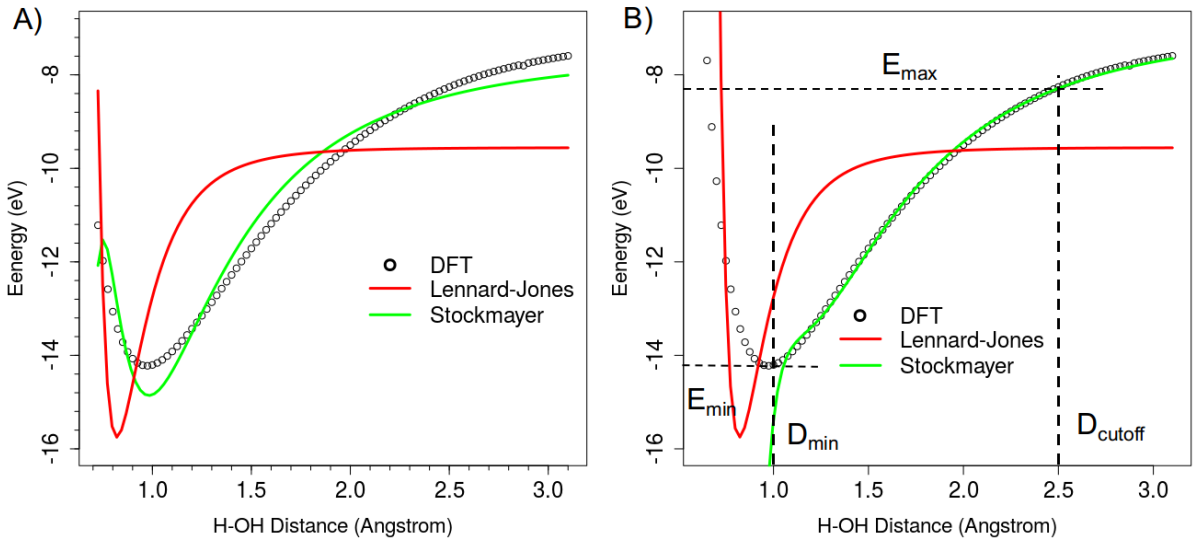

Figure S13: DFT calculated energies and fitting of Lennard-Jones and Stockmayer potentials.

4.5 Comparison of experiment parameter and parameter in our AIMD simulations

Table S9: Structural parameter in AIMD simulations and comparison to Ref. S17

	Atom-atom distance				Angle	Coordination number	
Models	Fe-Ni$_{out}$	Fe-Fe	Ni-Ni	Fe-O	Fe-O-Ni	Fe-Ni$_{out}$	Fe-O
Experiment	3.21-3.98	2.86-3.10	2.87-3.04	1.91-1.981-	67(90-23)	4-8,3-5	4.3-5.3
Normal H_2O							
2IN6	3.47-3.61		2.91-3.05	1.84-2.01	60-50	6	6
3IN6	3.47-4.06		2.86-3.10	1.84-2.40	49-70	6	6
BRIDGE	2.95-4.22	2.67	2.80-3.10	1.81-2.20	28-66	3-5	5
TILT	3.22-3.60	2.60	2.84-3.03	1.88-2.15	34-76	3	4-5
Excessive H_2O							
2IN6	3.55-4.18		2.80-3.10	1.88-2.07	50-60	6	6
3IN6	3.62-3.84		2.77-3.05	1.88-2.24	45-60	6	6
2UP	3.60-3.74		2.80-3.10	1.84-2.01	50-60	3	6
3UP	3.40-3.75		2.88-3.02	1.85-1.96	50-57	3	6
BRIDGE	3.33-3.75	3.15	2.84-3.01	1.83-2.20	53-72	5-6	6
TILT	3.49-3.65	3.44	2.83-3.10	1.86-2.10	49-65	3	3-5

4.6 Layer-layer distances

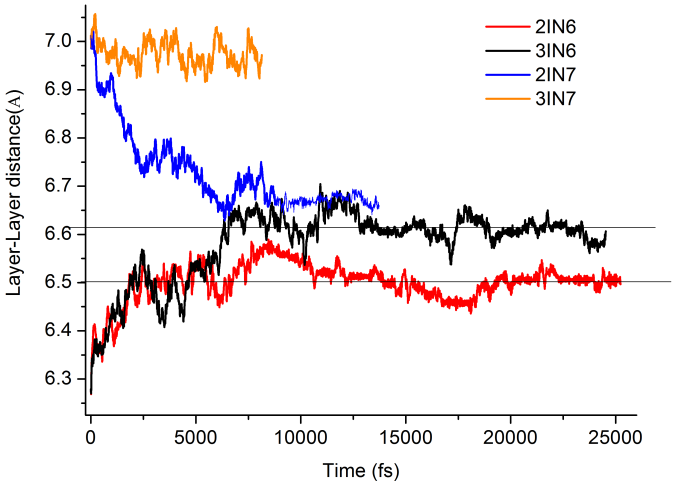

Figure S14: Layer-layer distances in 2IN6, 2IN7, 3IN6 and 3IN7 models. It shows D_{LL} of intercalation models with initial D_{LL} of 6 Å and 7 Å. After about 7 ps, the 2IN7 model narrows down and become similar to the 2IN6 model. But the 3IN7 model does not change due to the weak interaction of Fe^{3+} clusters, which agrees with its lower formation energy compared to Fe^{2+} clusters.

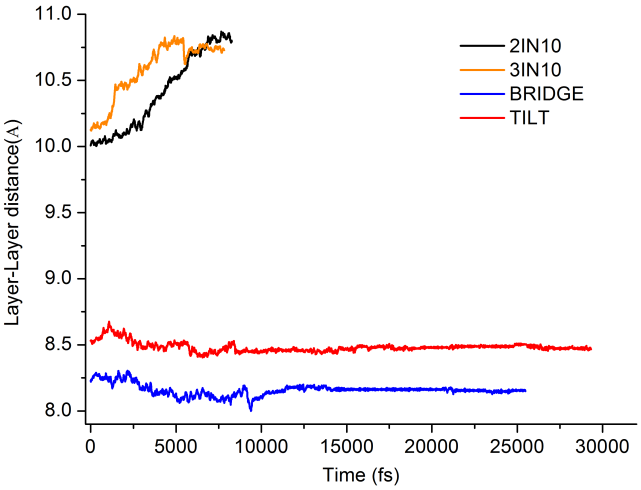

Figure S15: Layer-layer distance in 2IN10, 3IN10, BRIDGE and TILT models. The D_{LL} of 2IN10 and 3IN10 increase with time. At this case, these two model are equivalent to two surface models. The BRIDGE and TILT model show very stable D_{LL} after 10 ps.

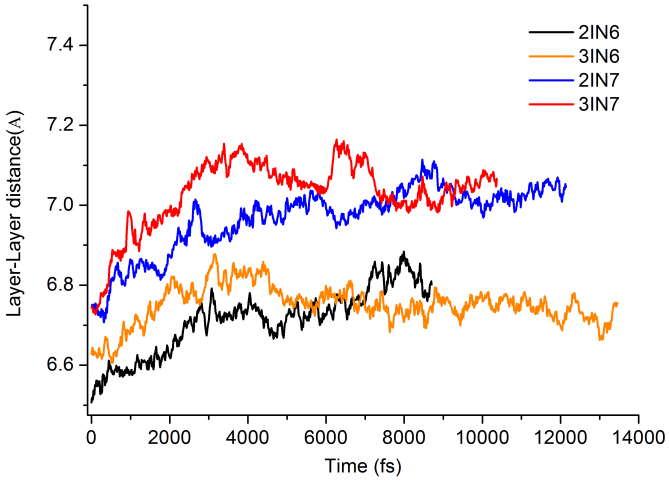

Figure S16: Layer-layer distance in 2IN6, 2IN7, 3IN6 and 3IN7 models with more water molecules. It displays the D_{LL} of intercalation models of 2IN6, 2IN7, 3IN6 and 3IN7 with more water molecules intercalated. Due to too much water molecules, the distance between all gaps increase.

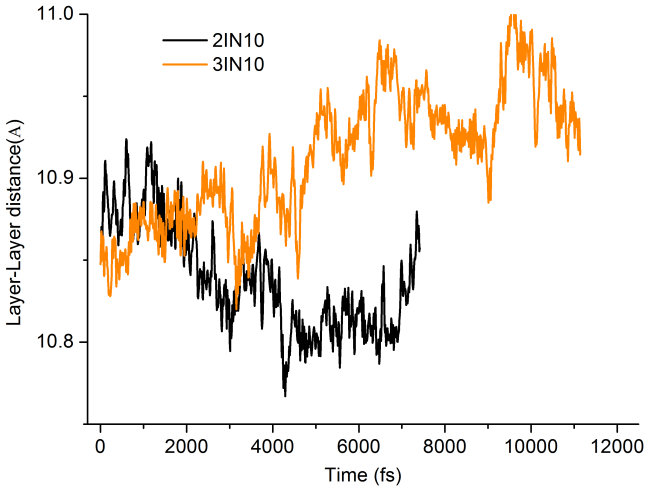

Figure S17: Layer-layer distance in 2IN10 and 3IN7 with more water molecules. It displays the D_{LL} of intercalation models of 2IN10 and 3IN10 with more water molecules intercalated. With more water molecule, these models become more stable than the model with fewer waters.

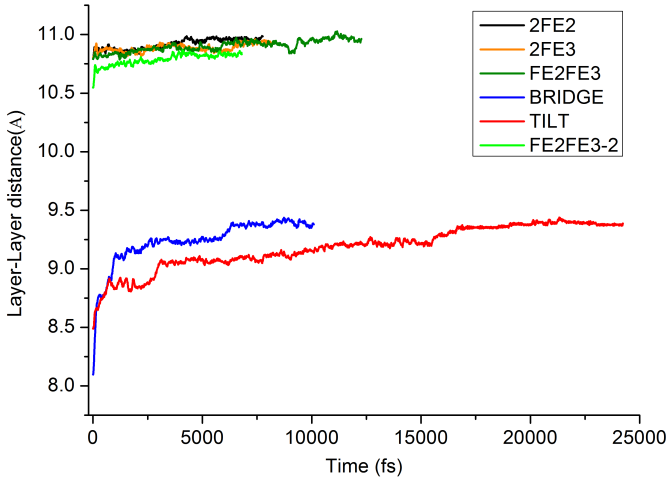

Figure S18: Layer-layer distance in intercalation models with more water molecules. It displays the D_{LL} of intercalation models of 2FE2 and 2FE3 with more water molecules intercalated. Their distances slowly increase. Although they look like stable, but we observed disconnection between Fe ions and NiOOH layers. The BRIDGE model get expanded, its Fe breaks one bond connect to the surface and then become TILT. While, if more water molecules are placed into the TILT model, the Fe ion will also break one bond connected to the oxygen that connects to the other Fe ion. At this case, the TILT model becomes 2FE2 or 2FE3. This also can be seen in their CN profile.

4.7 Oxidation states and coordination numbers

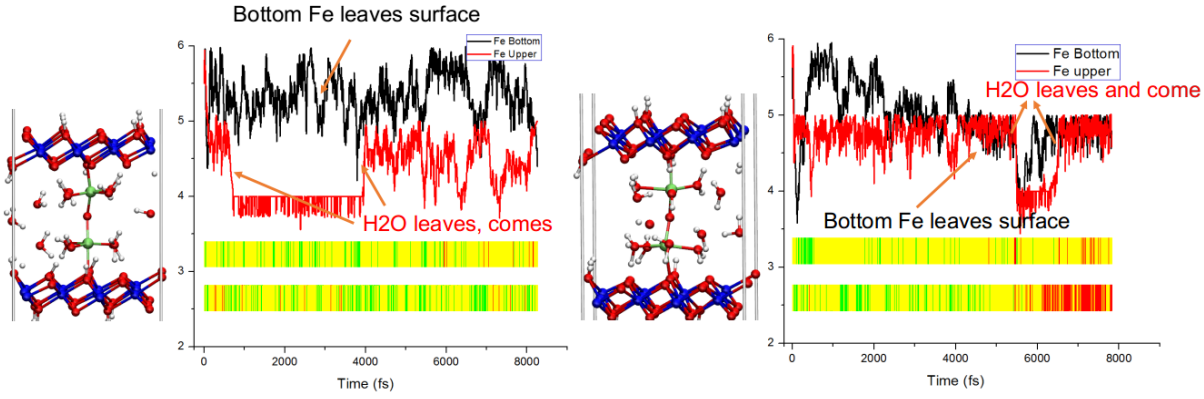

Figure S19: OS and CN of Fe ions in 2FE2 and 2FE3 models. Both of them are initial octahedrally coordinated, they both lose H_2O at the very beginning and the CNs become 5 or even 4. H_2O leaving can be clearly seen from the CN chart, but the OSs of these Fe ions are irreverent to H_2O leaving. Fe ions in these two models go away from the subsurface.

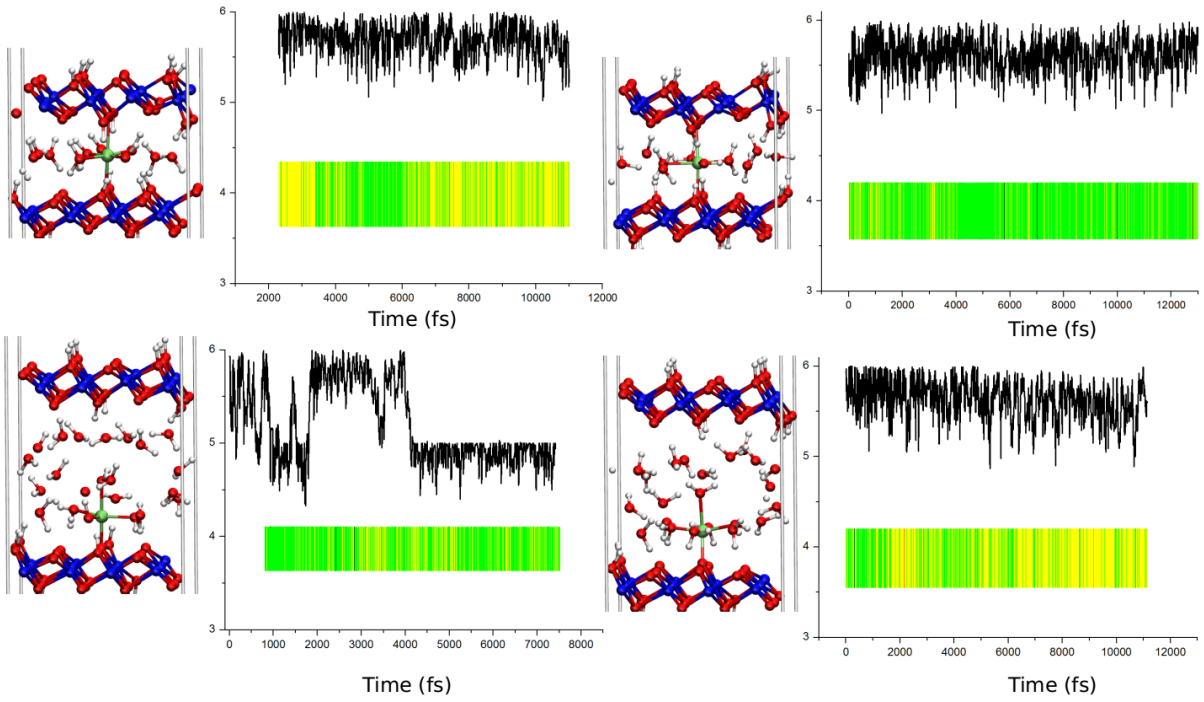

Figure S20: OS and CN of Fe ions in 2IN6, 3IN6, 2IN10 and 3IN10 with excessive H_2O molecules.

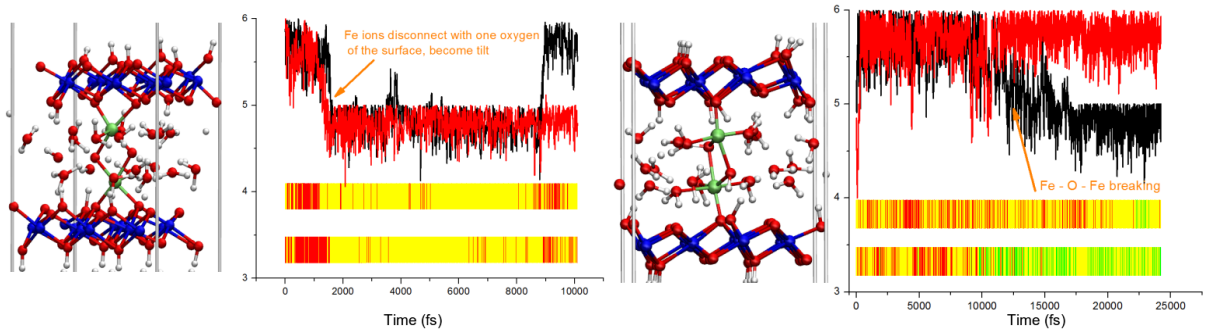

Figure S21: OS and CN of Fe ions in BRIDGE and TILT models with excessive water molecules. The Fe breaks one Fe-O bond with the surface at 1.7 ps in the BRIDGE model. After each Fe ion break one Fe-O with the surface, the BRIDGE model become the TILT model. If we add more water molecules in the TILT model, it will break the Fe-O bond between two Fe ions at 12 ps, and then become same with models of 2FE2 and 2FE3.

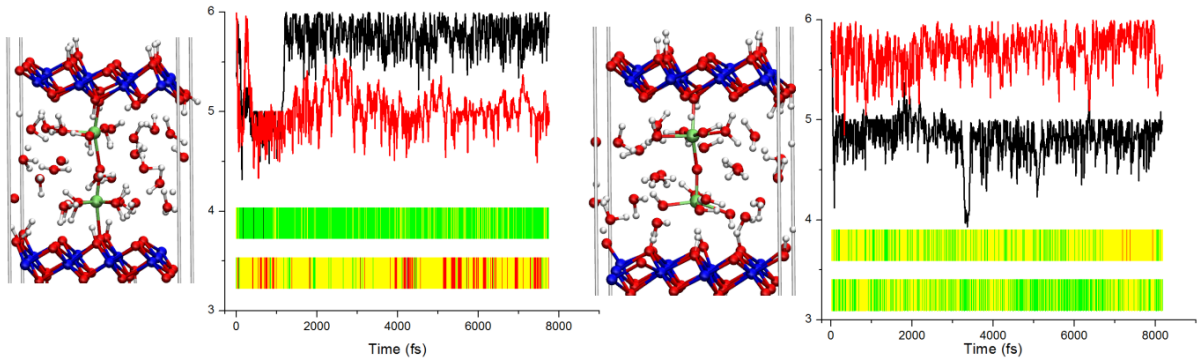

Figure S22: OS of Fe ions in 2FE2 and 2FE3 with excessive water molecules. The linking chain of O-Fe-O-Fe-O will break to make more space for excessive H_2O molecules.

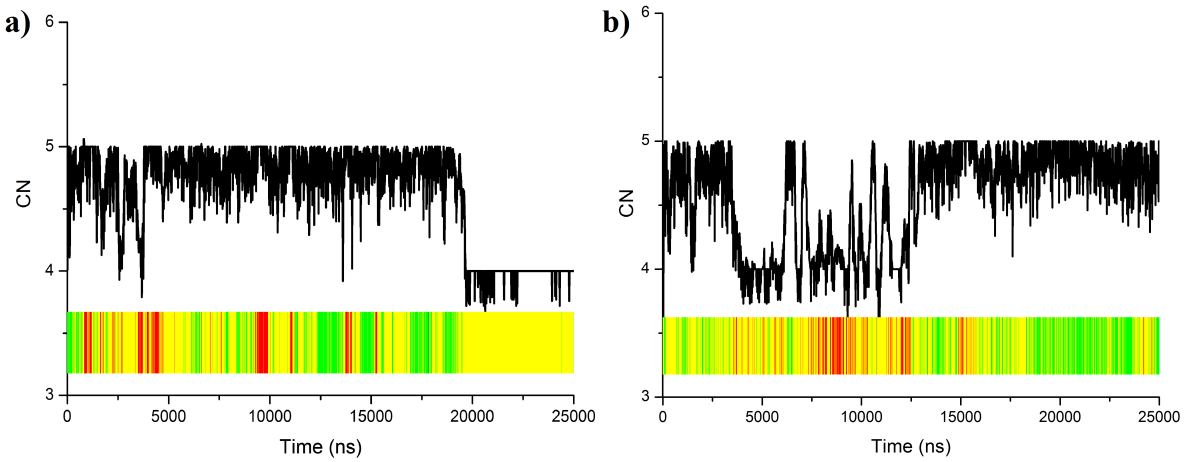

Figure S23: CN and OS of Fe ions in a) 2UP-Tetra and b) 3UP-Tetra models.

5 Possible configurations at reaction conditions

Although there are stable adsorption and intercalation models, in which different oxidation state Fe ions have been considered. At reaction conditions, the oxidation state of Fe ion should have a major form, for example, without any applied potential the most stable free Fe ion in water is Fe^{2+}, but it will be Fe^{3+} if the applied potential was higher than 0.56 V.[S18] The transition potential for the free Fe^{2+} going to Fe^{3+} is calculated to be 0.39 and 0.60 V for PBE+U and HSE06 calculations, respectively. The HSE06 result is almost the same to the experimental value of 0.56 V according to the CRC handbook.[S18] However, the PBE result is about 30% or 0.2 V lower than experiment.

Based on the reaction of $Sub{-}Fe^{2+}4{\cdot}H_2O{\cdot}OH^- \Leftrightarrow Sub{-}Fe^{3+}3{\cdot}H_2O2{\cdot}OH^- + H^+ + e^-$, we can determine when Fe^{2+} will transfer to Fe^{3+}. But actually a H of Fe cluster will

Table S10: Calculated free energy difference between Fe^{3+} and Fe^{2+}.

Models	Ions	E_0 (eV)	ZPE (eV)	ST (eV)	G (eV)	ΔG (eV)
Free ions (PBE+U)	Fe^{2+}	-85.264	3.399	0.370	-82.235	0.391
	$Fe^{3+} + H^+$	-84.609	3.070	0.304	-81.844	
Free ions (HSE06)	Fe^{2+}	-109.571	3.399	0.370	-106.542	0.510
	$Fe^{3+} + H^+$	-108.710	3.070	0.304	-106.032	
Adsorbed ions(PBE+U)	Fe^{2+}	-803.298	3.399	0.370	-800.269	1.699
	$Fe^{3+} + H^+$	-801.335	3.070	0.304	-798.569	

transfer to the substrate: $Sub{-}Fe^{2+}4 \cdot H_2O \cdot OH^- \Rightarrow H{-}Sub{-}Fe^{3+}3 \cdot H_2O2 \cdot OH^-$. The initial Fe^{2+} become Fe^{3+}. For the same reason, Fe^{3+} goes to Fe^{4+}. The transition potential for the 2UP model (Fe^{3+}) goes to the 3UP model (Fe^{4+}) is calculated to be 1.15 V based on PBE calculations. Considering the under estimation of PBE calculation for the free ions, we expect the transition potential in experiment should be about 1.50 V. Therefore, we conclude that both adsorbed Fe^{3+} and Fe^{4+} should be populated. Generally, at OER reaction conditions, the free iron ions are mainly in Fe^{3+}, but the adsorbed species are mainly Fe^{3+} and Fe^{4+}. This conclusion is consistent with our AIMD simulations.

Table S11: Free energy changes of reaction steps in all OER mechanisms

Models	Step1	Step2	Step3	Step4	Overpotential
Clean	0.526	1.339	1.883	1.172	0.653
2UP	0.767	1.455	1.240	1.457	0.227
2IN6	0.708	1.803	1.563	0.847	0.573
3UP	0.823	1.423	1.796	0.878	0.566
2IN6-Fe	1.423	1.849	1.661	-0.014	0.619
2UP-Fe-top	1.346	1.835	1.464	0.276	0.605
2UP-Fe-side	1.619	1.340	1.768	0.193	0.538
3UP-side	1.792	1.732	0.924	0.472	0.562
2UP-Fe-side-O2	1.619	1.340	0.948	1.013	0.389
TILT-Fe	0.696	2.007	0.871	1.346	0.777
BRIDGE*	1.819	0.475	1.129	1.496	0.589
Dimer-Fe2+-mid	1.042	1.742	1.429	0.706	0.512
Dimer-Fe2+-end	1.209	1.663	1.526	0.522	0.433
2UP-Tetra	0.846	0.900	1.721	1.453	0.491
3UP-Tetra	0.349	1.326	1.767	1.478	0.537

6 OER simulations

6.1 Energy profiles

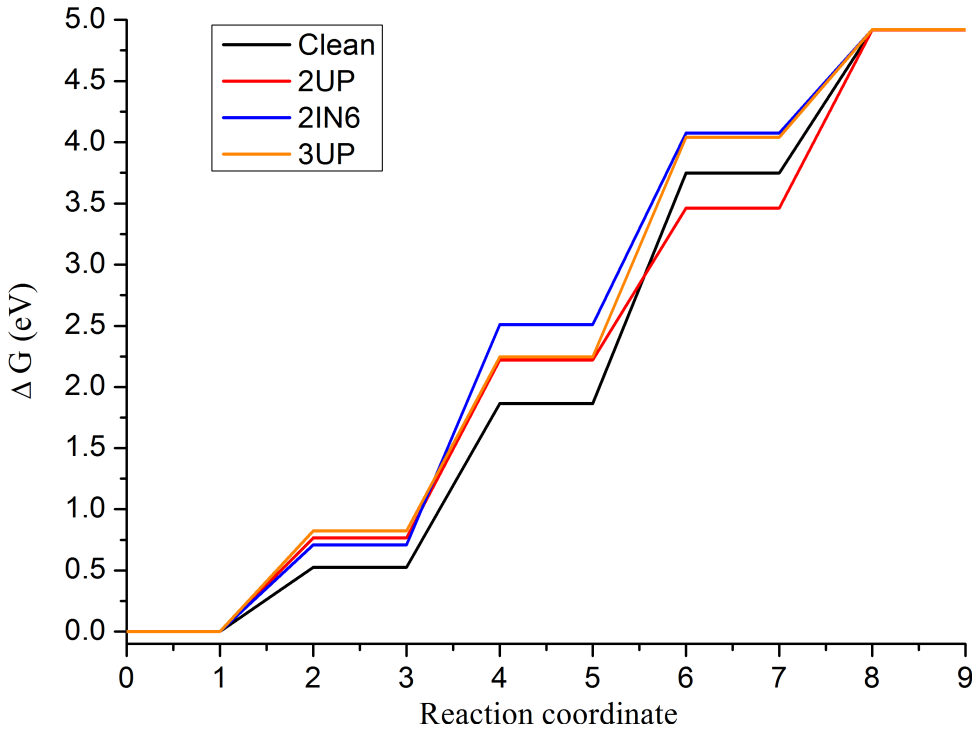

Figure S24: Energy profile of OERs with V_{OH}(Ni) as active site.

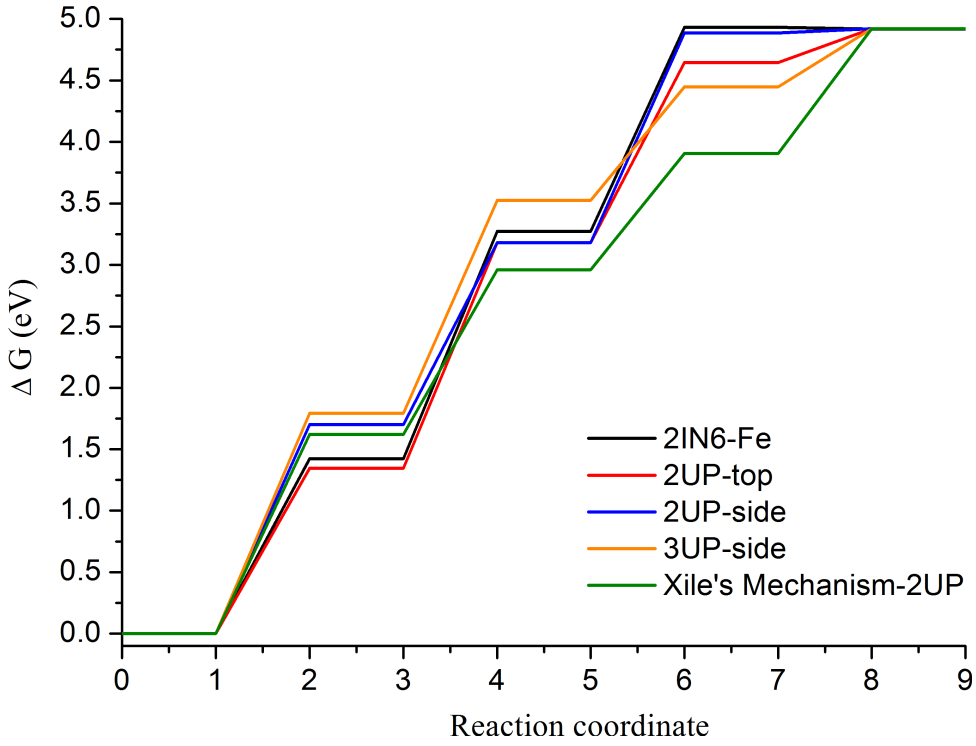

Figure S25: Energy profile of OERs with Fe as active site.

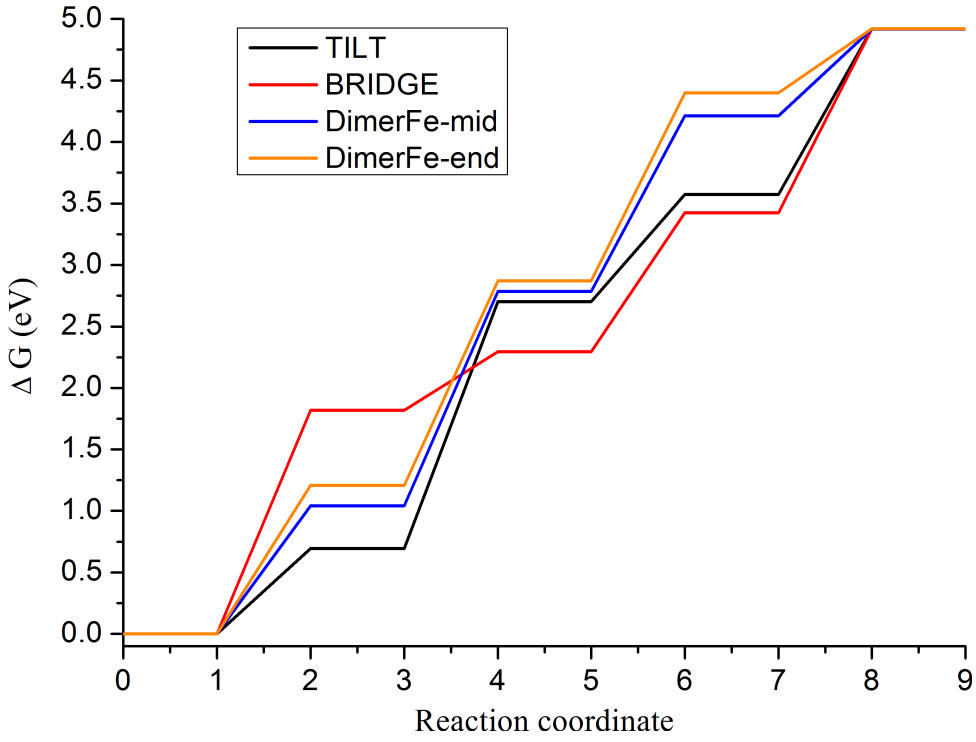

Figure S26: Energy profile of OERs with dimer Fe as active site.

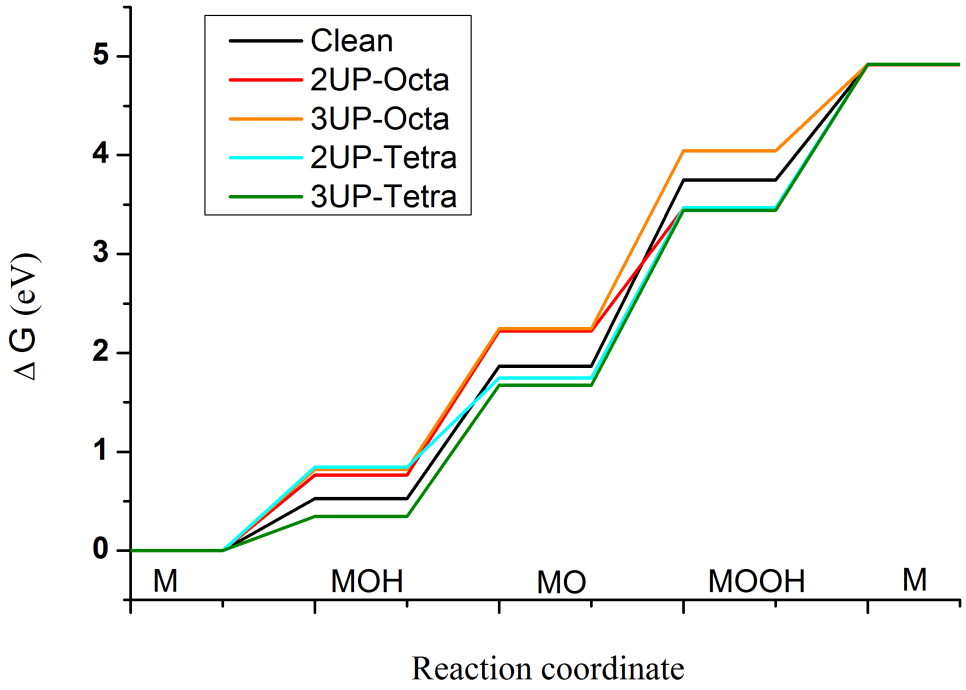

Figure S27: Energy profile of OERs in the octahedral and tetrahedral adsorption models.

Figure S24 demonstrates the energy profile of intermediates of OERs, in which Ni is active site. By adsorbing a Fe ion, the over potential reduces no matter the reaction site and the oxidation site of Fe ions. The over potential of a clean surface without Fe adsorption can be reduced from 0.65 V to 0.23 V by an adatom of Fe^{2+} ions, which is has the lowest overpotential in all OER mechanisms. Figure S25 shows the energy profile of OERs that Fe ions act as active site. The over potential for the 2IN6, 2UP-top, 2UP-side and 3UP-side are 0.62, 0.61, 0.54 and 0.56 V, respectively. The mechanism proposed in the Xile's paper indeed lowers the energy barrier by avoiding the formation of O-O band to 0.39 V. Figure S26 demonstrates OER mechanisms that two Fe ions were incorporated on/in surface and interface. The TILT model shows an overpotential of 0.77 V that is higher than the intrinsic clean surface. The high over potential is attributed to the high oxidation state of Fe ions in the model. For the OER occurs at the end of dimer Fe also shows a small over potential of 0.43 V. The rate determining step is removing a proton from OH^- coordinated to Fe ions. The reaction at the middle of two Fe ions is 0.51 eV, which is slightly higher than OER happens at the end position. Structures of intermediates and their magnetic order test are provided in the attached slides.

6.2 Bader charges, magnetic moments and OS of some ions in intermediates in OERs

We here give the Bader charge, magnetic moments (MM) and OS of some ions near the active site. Table S12 illustrated that information of OERs that occurs on the vacancy of an oxygen ion. The Bader charge of all metal ions varies within 0.2 $|e^-|$, however the MM and OS of Fe can be significantly altered. If we ceiling all the OS and MM into integer, the relationship between OS and MM is consistent with the crystal field theory for octahedral coordination. For example, the OS of M, MO, MOH and MOOH are +3, +4, +4 and +4, and then their MM are 5, 2, 4 and 4 μ_B. But there are problems for some intermediates, such as intermediates of 2IN6 model, the calculated OSs are about 1, while the MMs are about 5 μ_B. This is because when we calculated the OS, the substrate O raises +0.5 to each connected Fe ion (O is -2, four Fe ions are connected in total, then each raises +0.5). But actually each Fe-O(substrate) takes an electron, additionally, the relationship of OS and MM changes in different coordination environment. Therefore, the MM also can not be used to calculate the Fe OS in all cases.

Table S12: Bader charges and magnetic moments of ions, energy and total magnetic moment of intermediates in OERs with V_{OH} (Ni) as active site.

Mechanism	Intermediates	Bader Charge					Magnetic moment(μ_B)				OS_{Fe}
		O	Fe	Ni1	Ni2	Ni3	Fe	Ni1	Ni2	Ni3	
Clean	M	X	X	1.20	1.20	1.24	X	1.73	1.70	1.25	
	MO	-0.79	X	1.31	1.30	1.30	X	1.09	1.23	1.24	
	MOH	-1.06	X	1.26	1.30	1.30	X	1.75	1.31	1.31	
	MOOH	-0.51	X	1.25	1.29	1.29	X	1.74	1.31	1.30	
2UP-Ni	M	X	1.76	1.24	1.21	1.25	4.20	1.11	1.25	1.69	2.99
	MO	-0.78	1.59	1.31	1.30	1.30	-1.89	0.34	1.10	1.10	3.21
	MOH	-1.10	1.76	1.30	1.29	1.31	3.57	1.13	1.28	1.22	3.41
	MOOH	-0.53	1.74	1.28	1.29	1.29	-3.51	1.20	1.17	1.18	3.79
3UP-Ni	M	X	1.76	1.24	1.23	1.25	3.63	1.15	1.31	1.13	3.22
	MO	-0.80	1.75	1.30	1.28	1.31	-4.16	0.38	0.88	1.11	2.36
	MOH	-1.09	1.74	1.31	1.29	1.31	2.97	1.19	1.23	1.13	4.77
	MOOH	-0.52	1.72	1.28	1.25	1.29	-2.53	1.22	1.72	1.17	4.00
2IN6-Ni	M	X	1.75	1.24	1.24	1.21	-4.22	1.20	1.07	1.68	1.00
	MO	-0.74	1.76	1.28	1.31	1.30	-4.23	1.18	0.11	1.11	1.00
	MOH	-1.06	1.76	1.30	1.30	1.31	-4.22	1.22	1.07	1.10	1.00
	MOOH	-0.49	1.76	1.29	1.29	1.29	-4.21	1.20	1.09	1.23	0.79

Table S13: Bader charges and magnetic moments of ions, energy and total magnetic moment of intermediates in OERs with Fe as active site

Mechanism	Intermediates	Bader O	Bader Fe	MM(μ_B)	OS_{Fe}
2UP-Fe-TOP	M	X	1.66	-4.10	2.30
	MO	-0.66	1.66	3.30	3.20
	MOH	-1.14	1.74	-4.20	2.14
	MOOH	-0.48	1.74	4.14	2.19
2UP-Fe-Side	M	X	1.71	4.20	2.87
	MO	-0.76	1.67	-3.32	3.03
	MOH	-1.16	1.73	-4.21	2.05
	MOOH	-0.60	1.72	-4.17	2.08
2IN6-Fe	M	X	1.71	-4.16	1.58
	MO	-0.70	1.70	-3.33	2.85
	MOH	-1.05	1.77	3.80	2.62
	MOOH	-0.33	1.78	4.10	2.98
3UP-Fe-Side	M	X	1.70	-4.18	2.27
	MO	-0.55	1.66	2.37	3.93
	MOH	-1.19	1.73	-3.50	3.02
	MOOH	-0.22	1.73	3.99	3.19

Table S14: Bader charges and magnetic moments of ions, energy and total magnetic moment of intermediates in OERs with dimer-Fe as active site.

Mechanism	Intermediates	$Bader_O$	$Bader_{Fe1}$	$Bader_{Fe2}$	MM_{Fe1}	MM_{Fe2}	OS_{Fe1}	OS_{Fe2}
BRIDGE	M	X	1.69	1.68	3.53	-3.38	3.50	3.00
	MO	-0.34	1.68	1.69	3.40	-3.40	4.00	3.00
	MOH	-1.01	1.69	1.67	3.50	-3.36	4.00	3.00
	MH	X	1.69	1.68	3.50	-3.38	3.50	3.00
TILT-Fe	M	X	1.64	1.68	3.61	3.61	2.33	2.33
	MO	-0.77	1.66	1.65	3.32	-3.38	3.90	2.28
	MOH	-1.05	1.68	1.68	-3.36	3.54	3.10	2.32
	MOOH	-0.17	1.64	1.65	4.04	-3.33	4.19	2.19
Fe-Dimer-mid	M	X	1.67	1.70	4.17	4.19	2.60	2.55
	MO	-1.06	1.69	1.72	4.18	4.19	2.69	1.78
	MOH	-1.19	1.70	1.76	4.17	4.25	2.56	1.82
	MOOH	-0.58	1.72	1.74	4.11	4.20	2.69	2.84
Fe-Dimer-end	M	X	1.71	1.69	4.16	-4.15	3.29	2.14
	MO	-0.67	1.71	1.69	4.20	3.23	2.99	3.45
	MOH	-1.06	1.69	1.61	-4.19	-1.91	3.13	3.00
	MOO, H	-0.39	1.69	1.59	-4.18	-1.76	3.13	3.20

References

(S1) Chaput, L.; Togo, A.; Tanaka, I.; Hug, G. Phonon-phonon interactions in transition metals. *Phys. Rev. B* **2011**, *84*, 094302.

(S2) Tkalych, A. J.; Zhuang, H. L.; Carter, E. A. A Density Functional + U Assessment of Oxygen Evolution Reaction Mechanisms on β-NiOOH. *ACS Catal.* **2017**, *7*, 5329–5339.

(S3) Martirez, J. M. P.; Carter, E. A. Unraveling Oxygen Evolution on Iron-Doped β-Nickel Oxyhydroxide: The Key Role of Highly Active Molecular-like Sites. *J. Am. Chem. Soc.* **2019**, *141*, 693–705.

(S4) Li, Y.-F.; Selloni, A. Mechanism and Activity of Water Oxidation on Selected Surfaces of Pure and Fe-Doped NiO x. *ACS Catal.* **2014**, *4*, 1148–1153.

(S5) Elbaz, Y.; Caspary Toroker, M. Dual Mechanisms: Hydrogen Transfer during Water Oxidation Catalysis of Pure and Fe-Doped Nickel Oxyhydroxide. *Journal of Physical Chemistry C* **2017**, *121*, 16819–16824.

(S6) Eslamibidgoli, M. J.; Groß, A.; Eikerling, M. Surface configuration and wettability of nickel(oxy)hydroxides: a first-principles investigation. *Physical Chemistry Chemical Physics* **2017**, *19*, 22659–22669.

(S7) Wang, L.; Maxisch, T.; Ceder, G. Oxidation energies of transition metal oxides within the GGA+U framework. *Phys. Rev. B* **2006**, *73*, 195107.

(S8) Persson, K. A.; Waldwick, B.; Lazic, P.; Ceder, G. Prediction of solid-aqueous equilibria: Scheme to combine first-principles calculations of solids with experimental aqueous states. *Phys. Rev. B - Condens. Matter Mater. Phys.* **2012**, *85*, 1–12.

(S9) Beverskog, B.; Puigdomenech, I. Revised Pourbaix diagrams for nickel at 25-300 °C. *Corros. Sci.* **1997**, *39*, 969–980.

(S10) Mathew, K.; Sundararaman, R.; Letchworth-Weaver, K.; Arias, T. A.; Hennig, R. G. Implicit solvation model for density-functional study of nanocrystal surfaces and reaction pathways. *J. Chem. Phys.* **2014**, *140*, 084106.

(S11) Garcia-Ratés, M.; López, N. Multigrid-Based Methodology for Implicit Solvation Models in Periodic DFT. *J. Chem. Theory Comput.* **2016**, *12*, 1331–1341.

(S12) Martirez, J. M. P.; Carter, E. A. Effects of the Aqueous Environment on the Stability and Chemistry of β-NiOOH Surfaces. *Chem. Mater.* **2018**, *30*, 5205–5219.

(S13) Łodziana, Z.; Topsøe, N.-Y.; Nørskov, J. K. A negative surface energy for alumina. *Nat. Mater.* **2004**, *3*, 289–293.

(S14) Deng, J.; Nellist, M. R.; Stevens, M. B.; Dette, C.; Wang, Y.; Boettcher, S. W. Morphology Dynamics of Single-Layered Ni(OH)2/NiOOH Nanosheets and Subsequent Fe Incorporation Studied by in Situ Electrochemical Atomic Force Microscopy. *Nano Lett.* **2017**, *17*, 6922–6926.

(S15) Hutter, J.; Iannuzzi, M.; Schiffmann, F.; VandeVondele, J. <scp>cp2k:</scp> atomistic simulations of condensed matter systems. *Wiley Interdiscip. Rev. Comput. Mol. Sci.* **2014**, *4*, 15–25.

(S16) Walsh, A.; Sokol, A. A.; Buckeridge, J.; Scanlon, D. O.; Catlow, C. R. A. Oxidation states and ionicity. *Nat. Mater.* **2018**, *17*, 958–964.

(S17) Song, F.; Busch, M. M.; Lassalle-Kaiser, B.; Hsu, C.-s.; Petkucheva, E.; Bensimon, M.; Chen, H. M.; Corminboeuf, C.; Hu, X. An Unconventional Iron Nickel Catalyst for the Oxygen Evolution Reaction. *ACS Cent. Sci.* **2019**, *5*, 558–568.

(S18) Haynes, W.; Bruno, T.; Lide, D. *CRC Handbook of Chemistry and Physics: A Ready-reference Book of Chemical and Physical Data*; CRC Handbook of Chemistry and Physics; CRC Press, 2014.